Universiteit Antwerpen

This item is the archived peer-reviewed author-version of:

Vapor nanobubble is the more reliable photothermal mechanism for inducing endosomal escape of siRNA without disturbing cell homeostasis

Reference:
Fraire Juan C., Houthaeve Gaëlle, Liu Jing, Raes Laurens, Vermeulen Lotte, Stremersch Stephan, Brans Toon, Garcia Alfonso Gerardo, De Keulenaer Sarah, Van Nieuw erburgh Filip, ...- Vapor nanobubble is the more reliable photothermal mechanism for inducing endosomal escape of siRNA w ithout disturbing cell homeostasis
Journal of controlled release - ISSN 0168-3659 - 319(2020), p. 262-275
Full text (Publisher's DOI): https://doi.org/10.1016/J.JCONREL.2019.12.050
To cite this reference: https://hdl.handle.net/10067/1653770151162165141

uantwerpen.be
Institutional repository IRUA

Vapor Nanobubble is the more reliable photothermal mechanism for inducing endosomal escape of siRNA without disturbing cell homeostasis.

Juan C. Fraire,[1] Gaëlle Houthaeve,[1,2] Jing Liu,[1] Laurens Raes,[1] Lotte Vermeulen,[1] Stephan Stremersch,[1] Toon Brans,[1] Gerardo García-Díaz Barriga,[2] Sarah De Keulenaer,[3] Filip Van Nieuwerburgh,[4] Riet De Rycke,[5,6] Jo Vandesompele,[7] Pieter Mestdagh,[7] Koen Raemdonck,[1] Winnok H. De Vos,[2] Stefaan De Smedt,[1] Kevin Braeckmans,[1,8]*

[1]Laboratory for General Biochemistry and Physical Pharmacy, Faculty of Pharmaceutical Sciences, Ghent University, Ghent, Belgium

[2]Laboratory of Cell Biology and Histology, Department of Veterinary Sciences, University of Antwerp, Antwerp, Belgium

[3]NXTGNT, Faculty of Pharmaceutical Sciences, Ghent University, Ghent, Belgium

[4]Laboratory of Pharmaceutical Biotechnology, Faculty of Pharmaceutical Sciences, Ghent University, Ghent, Belgium

[5]Center for Inflammation Research, VIB, Ghent, Belgium and Department of Biomedical Molecular Biology, Ghent University, Ghent, Belgium

[6]Center for Plant Systems Biology, VIB, Ghent, Belgium and Department of Plant Biotechnology and Bioinformatics, Ghent University, Ghent, Belgium

[7]Center for Medical Genetics, Ghent University, Ghent, Belgium

[8]Université de Lille, IEMN UMR 8520 and Lab. Phys. Lasers Atomes & Mol. UMR 8523, Villeneuve d'Ascq, France

*Corresponding author: kevin.braeckmans@ugent.be

ABSTRACT

Strategies for controlled delivery of therapeutic macromolecules into living cells, such as siRNA for reducing endogenous gene expression, are on high demand. Unfortunately, endosomal escape remains the most prominent bottleneck at the intracellular level for non-viral vectors today. The photothermal properties of gold nanoparticles (AuNP) can be used to overcome the endosomal membrane barrier upon laser irradiation. Depending on the energy of nanosecond laser pulses, two distinct photothermal mechanisms can be generated: endosomal rupture by mechanical energy from water vapor nanobubbles (VNBs) that emerge around the AuNP, or permeabilization of the endosomal membrane by heat diffusion. Here, we address the open question of how both photothermal effects influence cargo release, transfection efficiency, acute cytotoxicity and cell homeostasis. After developing a siRNA/AuNP drug delivery system, we found that the *in vitro* release of siRNA from the AuNP carrier occurs equally efficiently by VNB formation or heat generation. After uptake into cells, we discovered that the laser energy needed to generate either of both photothermal effects had decreased by accumulation in the same endosomes. The extent to which this happened was cell type dependent, showing that laser parameters need to be optimized to induce a particular photothermal effect. Heat-mediated endosomal escape happened more efficiently in those cells that had more particles per endosome, resulting in variable siRNA transfection results (20-50% downregulation) for different cell types. In contrast, VNB-mediated endosomal escape did not dependent on the number of AuNP per endosome, yielding high transfection efficiency (50-60% downregulation) independent of the cell type. When looking into the effects of photothermal endosomal escape on cell homeostasis by whole transcriptome analysis, more dysregulated genes were found after 6h for VNB as compared to heat-mediated endosomal escape. However, cell homeostasis recovered quickly and was not significantly affected after 24h or 48h for either of both photothermal mechanisms. Overall, we conclude that VNB-mediated endosomal escape is the more consistent photothermal effect to induce efficient endosomal escape and gene silencing independent of the cell type without long lasting effects on cell homeostasis.

KEYWORDS

gold nanoparticles, endosomal escape, vapor nanobubbles, intracellular delivery, siRNA, transfection, photoporation, transcriptomics.

INTRODUCTION

Nanoparticulate drug delivery systems (DSS) are nowadays actively used for the delivery of therapeutics into cells, such as short interfering RNA (siRNA) for hereditary disorders,[1] DNA for gene therapy,[2] antigens for vaccines,[3] and proteins for anticancer treatment[4]. DDS face the major challenge of trying to control where the encapsulated therapeutic cargo is trafficked to, once the DDS is taken up by the target cells. DDS uptake into cells typically happens via endocytosis, after which they are trafficked along the endocytic pathway, eventually ending up primarily in the acidic lysosomal compartments.[5] This acidic environment can result in significant degradation of the therapeutic cargo, resulting in reduced efficiency (Scheme 1A). Therefore, the therapeutic molecule must be able to escape from the endocytic vesicles into the cytoplasm, preferably before reaching the endolysosomes. Many strategies for achieving endosomal escape are based on effects induced by the composition or the functionalization of the DDS, such as the proton sponge effect and osmotic lysis, membrane fusion, membrane disruption or pore formation.[5] However, in spite of decades of DDS development for the delivery of biopharmaceuticals, achieving efficient endosomal escape remains one of the major bottlenecks for intracellular drug delivery today.[5–7]

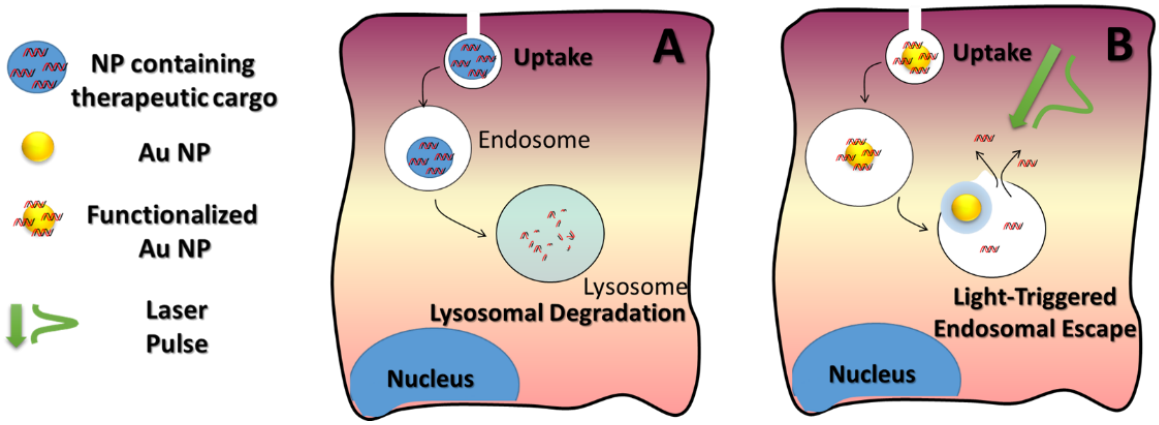

Scheme 1. A) Drug delivery systems are taken up by endocytosis and trafficked to the acidic endo-lysosomes where they run the risk of being degraded without exerting their therapeutic effect. B) Plasmonic nanoparticles have the ability to disrupt the endosomal membrane upon light irradiation and release the therapeutic molecules into the cytoplasm.

Due to the low endosomal escape efficiency of chemical based methods, physical approaches for the direct delivery of drug molecules into the cytoplasm have been proposed instead, especially for generating engineered cells *in vitro* and *ex vivo*.. Methods like electroporation, sonoporation, cell squeezing and laser-induced photoporation all use physical forces to generate transient pores in the cell membrane allowing exogenous materials to diffuse directly into the cell's cytoplasm.[8] While these strategies circumvent the problem of endosomal escape by avoiding endocytic uptake altogether, their major drawback is that a high concentration (typically micromolar range) of the cargo molecules is needed in the cell medium to create a sufficiently large concentration gradient. This quickly becomes problematic for expensive compounds like mRNA, nanobodies, CRISPR/CAS nucleoprotein complexes, etc.

As a trade-off, DDS have been suggested that are still taken up by endocytosis but that can induce endosomal escape based on a physical trigger. This way, advantages of both worlds are combined, i.e. a low amount of cargo needed (nanomolar range) due to efficient DDS endocytosis in cells combined with the controllability of physical stimuli that can efficiently induce endosomal escape on demand. In particular, DDS have been developed that contain AuNPs for light-triggered endosomal escape through the generation of photothermal effects (Scheme 1B). Examples are drug-loaded liposomes functionalized with AuNPs,[9,10] or the use of AuNPs as nanocarriers onto which the therapeutic agent is loaded.[11–15] For instance, recent studies have shown that siRNA-loaded AuNPs can induce 40% of GFP silencing in H1299 GFP lung cancer cells following irradiation with continuous wave (CW) laser light,[11] while 80 % of GFP silencing was reported in C116 mouse cells when irradiated with 130 fs laser pulses.[12] Other work focused on the killing of cancer cells with AuNPs loaded with siRNA or proteins irradiated with laser pulses that range from 0.1 ps to 5 ns.[13–15] While these initial studies show that the concept of light-triggered

endosomal escape using AuNP is promising, the underlying mechanism remains unclear, especially since different laser irradiation conditions have been used which can induce fundamentally different photothermal effects. It is well known that AuNPs have an enhanced absorption cross-section[16] and that they first dissipate the absorbed light energy to the atomic lattice via electron−phonon interactions causing the AuNP temperature to increase.[17] If the energy transferred to the surrounding fluid is sufficiently high, a vapor layer can be formed at the AuNP surface which expands as a bubble, and subsequently collapses on the sub-microsecond time scale.[17,18] The formation of these vapor nanobubbles (VNB) is a distinct photothermal phenomenon in which almost all light energy is converted to mechanical energy (expansion and collapse of the VNB) with negligible heating of the environment (i.e. a purely mechanical effect).[19] Instead, when the energy is not enough to induce VNB formation, the relaxation occurs by heat diffusion into the surrounding medium (heating effect). Up to this point it remains unknown which of both distinct effects is the most advantageous to achieve the best endosomal escape and cell transfection when using AuNP nanocarriers. In addition, while acute toxicity is often measured in transfection studies, a detailed comparison of how either of both photothermal mechanisms influence cell homeostasis over time is currently missing.

Here, we aimed to answer these open questions on light-triggered endosomal escape with AuNP carriers for siRNA transfections. A systematic comparison was carried out of the VNB and heating regime, with the goal of providing insight into which of these mechanisms favor siRNA release, endosomal escape, transfection efficiency, cell viability and cell homeostasis. We found that the laser fluence needed for generating heat or VNB is affected by the AuNP concentration and endosomal maturation stage in a cell-dependent manner. Our results furthermore showed that VNB-mediated endosomal escape produces reproducible siRNA transfections independent of the cell type, while the performance of heat-mediated endosomal escape is dependent on the degree of clustering of AuNPs inside the endosomes of a particular cell type. A detailed comparison on the effect of both regimes on the cell's transcriptome revealed that, even though VNB is a more drastic nanoscale event compared to heat diffusion, it did not elicit a stronger activation of programmed cell death or DNA repair pathways as

compared to the heating regime. Compared to the untreated control, however, both regimes showed some genes involved in these pathways to be differentially expressed. Nevertheless, this did not result in a unilateral response, since no significant activation nor inhibition of programmed cell death and DNA repair pathways was found. Together our results point towards VNB-mediated endosomal escape strategy as the more reproducible endosomal escape and gene silencing method, without compromising cell viability or long-term cell homeostasis.

RESULTS

Synthesis and characterization of siRNA loaded AuNP nanocarriers.

The main goal of this study is to obtain a deeper understanding of the capabilities and limitations of light-triggered endosomal escape strategies using AuNP carriers as the source of the photothermal phenomenon responsible for disrupting the endosomal membrane. To this end, we designed an AuNP carrier for siRNA delivery with a typical size of around 0.1 μm. AuNPs of 95 nm were obtained by the Turkevich synthesis method,[20] and functionalized following a polyelectrolyte strategy (Figure 1A). The experimental extinction spectrum is shown in Figure 1B and matches with the expected spectrum as calculated by Mie theory simulations for 95 nm AuNP. Further confirmation of the size was obtained by DLS (Figure 1C) and TEM (Figure 2B). Notice that the absorption component of the total extinction is maximal at the laser wavelength used in this study (λ = 561 nm).

After synthesis, to stabilize the AuNPs, they were first coated with hyaluronic acid (HA - a negatively charged polymer), and subsequently functionalized with a positively charged polymer, poly(diallyl dimethyl ammonium chloride) (PDDAC). PDDAC is known to have negligible cytotoxicity[21] and gives a net positive charge to the NPs which is independent of the pH (quaternary amino group), allowing to further load the carrier with siRNA molecules by electrostatic interactions. Successful functionalization with PDDAC and subsequent siRNA loading was confirmed by the charge reversal as determined by zeta potential measurements (See Figure 1C and Figure S1A). To examine the binding efficiency of the siRNA with the PDDAC/HA/AuNP carriers, we performed agarose gel electrophoresis

measurements. The results shown in Figure S1B indicate successful complexation of siRNA up until ~1700 siRNA molecules per carrier. At double the concentration a small fraction of siRNA was no longer complexed, indicating saturation of siRNA complexation onto the carriers. Therefore, the formulation with ~1700 siRNA molecules per carrier was selected for all further experiments.

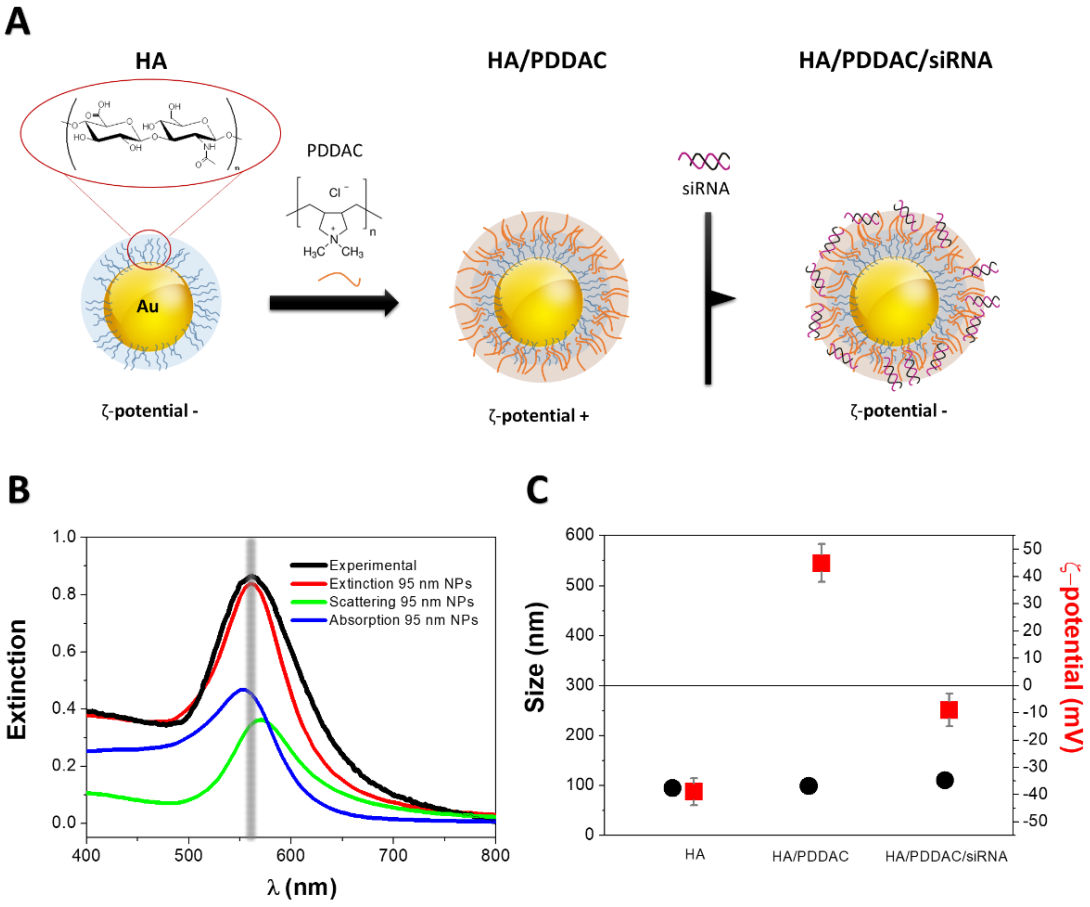

Figure 1. Design and characterization of cationic AuNP loaded with siRNA. A) AuNPs were functionalized with hyaluronic acid (HA), followed by functionalization with poly(diallyl dimethyl ammonium chloride) (PDDAC), a positively charged polymer for electrostatic loading of the negatively charged siRNA. B) Experimental extinction spectrum of synthesized AuNPs and simulated extinction, absorption and scattering cross-sections of spherical 95 nm AuNPs. The grey line represents the irradiation wavelength of 561 nm used in this study. C) Physicochemical characterization by dynamic light scattering and zeta potential of the nanocarriers during the different functionalization steps.

Carrier desintegration upon pulsed laser irradiation in the heating or VNB regime.

Using nanosecond laser pulses, one can selectively induce either heat or VNBs by tuning the laser pulse fluence,[19] which is the incident energy per unit area. We first determined the laser energy level needed to generate VNBs. The formation of VNBs can be detected by dark-field microscopy through a sudden increase of scattered light at the location where they are formed. A suspension of AuNP carriers was irradiated by individual 7 ns laser pulses of increasing energy and the number of VNBs that appear in the laser irradiation spot was counted (~150 μm laser beam diameter) (See Figure S2). As the laser energy increases, more VNBs are formed, finally saturating when the maximum number of AuNPs in the laser spot generate VNBs (Figure 2A). The VNB threshold is commonly defined as the fluence level (J/cm²) needed at which 90% of the maximal number of VNBs is obtained.[18] The VNB threshold for the 95 nm AuNP carriers was found to be 1.25 J/cm². The heating regime can then be defined by the laser fluence at which there is only low probability of VNB generation. Here we selected the 10% probability level, corresponding to a fluence of 0.23 J/cm².

Having established the laser fluence levels needed to either generate heat or VNB from the AuNP nanocarriers, we proceeded with characterizing the AuNP and cargo integrity after irradiation with a single laser pulse. Figure 2B shows the TEM characterization of the AuNP carrier before laser irradiation. The average size determined by TEM analysis was (91 ± 22) nm, in good agreement with the previously estimated size of 95 nm. The AuNPs after laser irradiation are shown in Figures 2C and D for VNB and heating, respectively. At high laser fluence to generate VNBs, AuNPs fragmented into small pieces of 6 nm on average, an observation that has been reported before.[22–24] The corresponding extinction spectrum (Figure S3A) matches with the simulated spectrum of 8 nm AuNPs, in close agreement with the TEM results. At lower laser fluence to induce heating, the fragmentation is less drastic and ~3 different populations can be observed centered at 10 nm, 30 nm and 60 nm (See histogram in Figure 2D). The simulated extinction spectrum for those three fractions combined matches closely with the experimental one, further confirming the TEM results (Figure S3B).

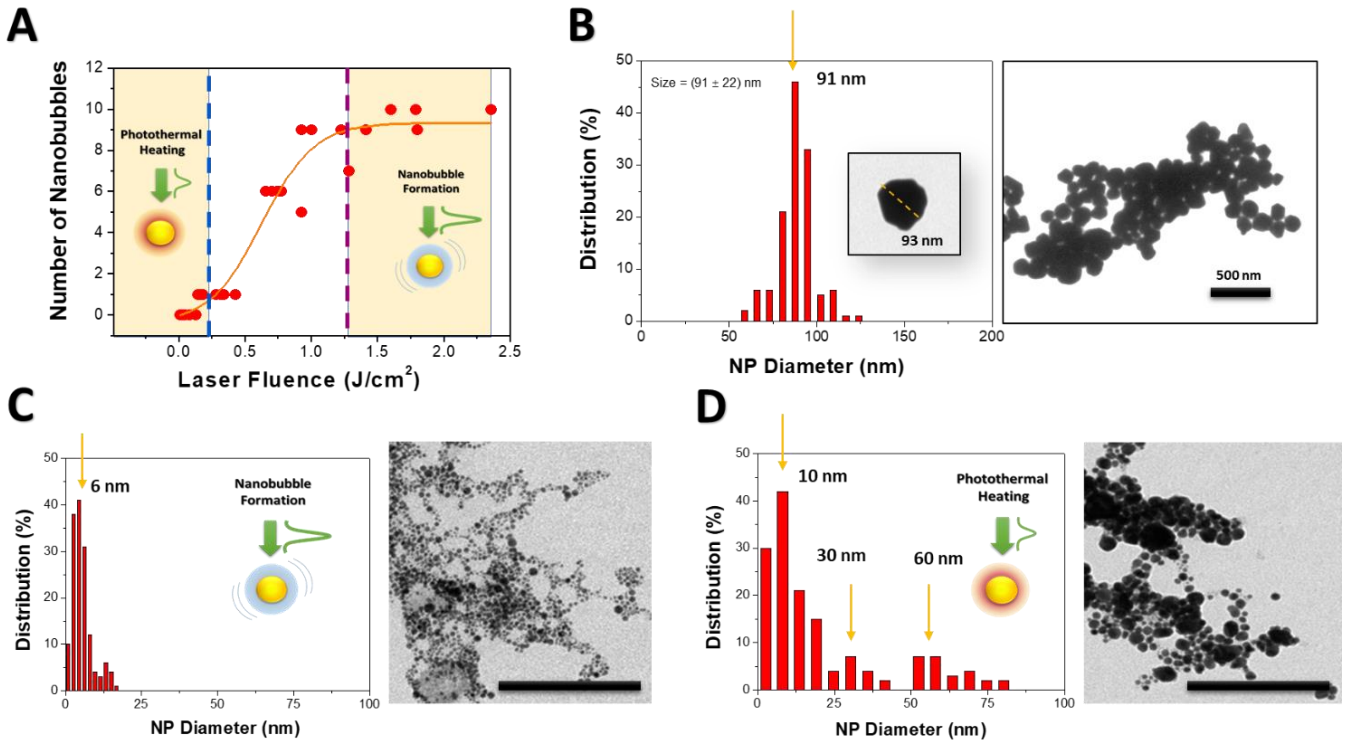

Figure 2. Effect of irradiating the AuNP nanocarriers with a 7 ns laser pulse in the VNB and heating regime. (A) Determination of the vapor nanobubble (VNB) fluence threshold. The heating and VNB regimes are highlighted in the graph. (B) Size distribution of AuNPs determined by TEM analysis. (C) TEM analysis of AuNPs after irradiation with one laser pulse at a laser fluence corresponding to the VNB threshold (1.25 J/cm²). (D) TEM analysis of AuNPs irradiated with one laser pulse at a laser fluence in the heating regime (0.23 J/cm²). The size distributions were obtained after analysis of at least 500 NPs in all cases. The scale bars in (C) and (D) indicate 200 nm.

siRNA release and integrity upon irradiation in the heating or VNB regime.

The observed particle fragmentation leads to the question if the siRNA cargo at the surface remains intact after inducing either of both photothermal effects. Figure 3A shows a gel electrophoresis run of siRNA loaded PDDAC/HA/AuNP carriers after irradiation with a single laser pulse in the heating or VNB regime. In both cases a band can be seen near the bottom of the gel at the expected place for siRNA, showing that at least part of the siRNA is released. Based on a fairly identical intensity of the bands it

seems that siRNA is released to a similar extent by heating or VNB generation. As the bands did not become more intense after addition of dextran-sulfate to displace any remaining siRNA from the particles, we conclude that no intact siRNA remains on the particles after laser irradiation. To further check if some of the released siRNA may be degraded, we additionally performed micro gel electrophoresis runs, showing that the siRNA remains intact (21 base pairs) and is released to the same extent for both laser regimes (See Figure 3B).

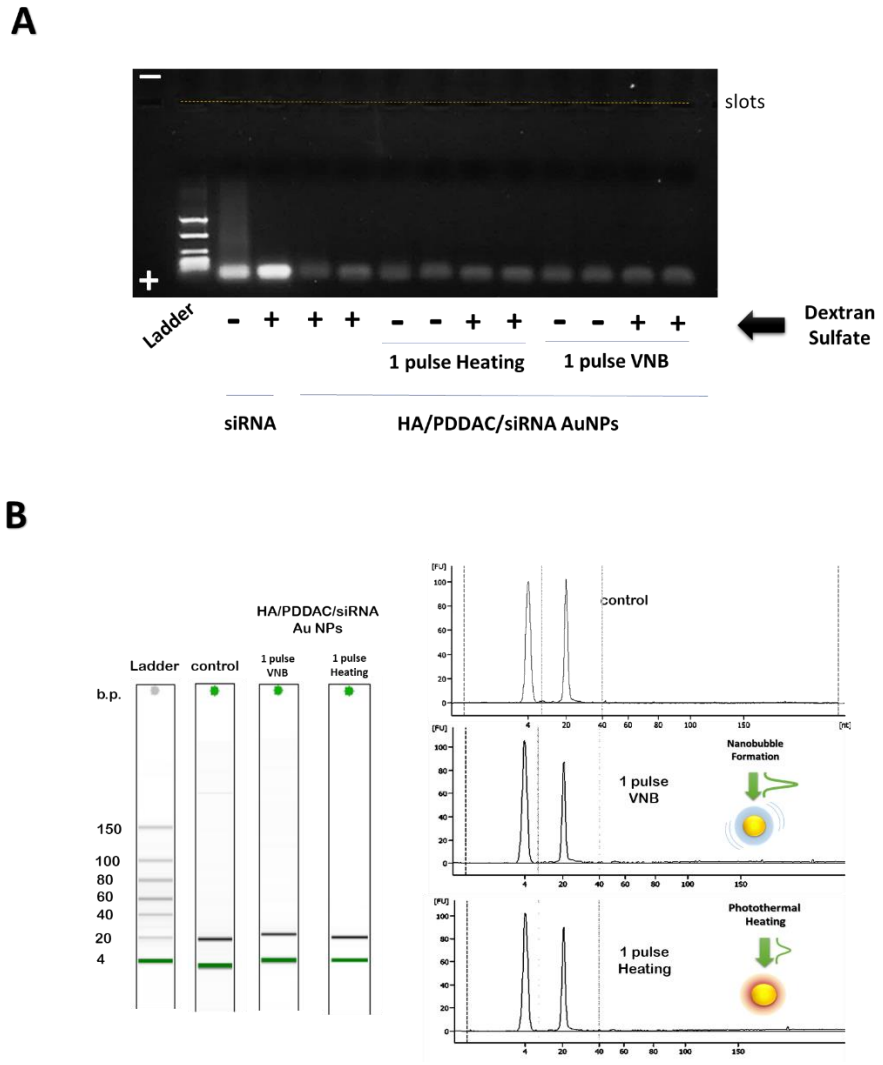

Figure 3. Laser induced release of siRNA from PDDAC/HA/AuNP carriers. (A) Gel electrophoresis run after irradiation with a single laser pulse in the heating or VNB regime. Plus and minus signs indicate whether or not dextran sulfate was added after laser irradiation. Heating and VNB, do not show significant

differences with respect to the controls (irradiated and non-irradiated) after addition of dextran sulfate (10 μg/mL) to induce siRNA release, indicating that most of the cargo is released upon irradiation. Experiments were performed in duplicate. (B) AuNP carriers loaded with siRNA were irradiated with a single laser pulse in the VNB or heating regime. siRNA was analyzed on an Agilent μgel electrophoresis chip, providing that the siRNA is not fragmented by a single laser pulse in the heating or VNB regime.

Effect of endosomal sequestration on the required laser fluence for heating or VNB generation.

Successful uptake of PDDAC/HA/AuNP nanocarriers loaded with siRNA (siRNA/AuNP) was studied in two different cell types, H1299 cells expressing green fluorescence protein (H1299 GFP)[25] and stably transfected HeLA cells expressing GFP coupled to a nuclear localization signal (HeLa NLS-GFP).[26] Note that GFP expressing cell lines were chosen to quantify siRNA mediated gene silencing further on. Intracellular uptake was quantified by confocal microscopy and flow cytometry making use of siRNA labeled with Alexa Fluor 647 (AF647 siRNA). Figure S4A shows a representative microscopy image of HeLa's and H1299's after 1 h incubation with siRNA/AuNP at $1.5x10^8$ NPs/mL. The AuNP core, visualized in confocal reflection mode, colocalizes perfectly with the red signal coming from AF647 siRNA, indicating that the siRNA and AuNP carriers are present together in the same endosomes. Flow cytometry showed that siRNA/AuNP are well taken up by both cell types to a similar extent (Figure S4B). The absence of signal when siRNA/AuNP were incubated at 4°C (inhibition of endocytic processes) confirms active endocytic uptake at 37°C.

Since particles are taken up by endocytosis, we checked if this may have changed the VNB generation threshold. Indeed, it is known that the VNB threshold may change upon clustering of AuNPs,[27] which can happen if multiple particles reside within the same endosome. As before, the number of VNBs was quantified by dark field microscopy for an increasing laser fluence after 1h incubation of siRNA/AuNP in both HeLa NLS-GFP and H1299 GFP cells. A representative dark field image is shown in Figure 5A of HeLa NLS-GFP cells before and during VNB formation. The data in Figure 5B reveal

that there is a substantial difference in the VNB threshold between both cell types. The VNB threshold in H1299 GFP cells was ~0.06 J/cm², while for HeLa NLS-GFP it was ~0.21 J/cm², which is 17× and 5× less than for AuNP dispersed in water, respectively. Similarly, the threshold for heating was determined to be ~0.02 J/cm² for H1299 GFP cells, while for HeLa NLS-GFP it was ~0.12 J/cm², which is 13.5× and 2.2× less than for AuNP dispersed in water, respectively. This cell type dependency was further confirmed by including unmodified HeLa's as a third cell type, which showed a higher VNB threshold (~0.48 J/cm²) than HeLa NLS-GFP cells and H1299 GFP cells. In order to better understand these differences, we performed TEM analysis of the uptake of siRNA/AuNP in HeLa NLS-GFP cells and H1299 GFP cells (Figure 5C). Analysis of the NP-containing endosomes revealed that H1299 GFP cells have on average ~17 AuNPs/endosome while in HeLa NLS-GFP cells this was significantly lower at ~7 AuNPs/endosome. A lower VNB and heating threshold in H1299 GFP cells can thus be understood from a higher degree of particle clustering in endosomes.[27] Together our results clearly show for the first time that endocytic uptake can have a marked influence on the laser fluence needed for VNB or heat generation in a highly cell-dependent manner.

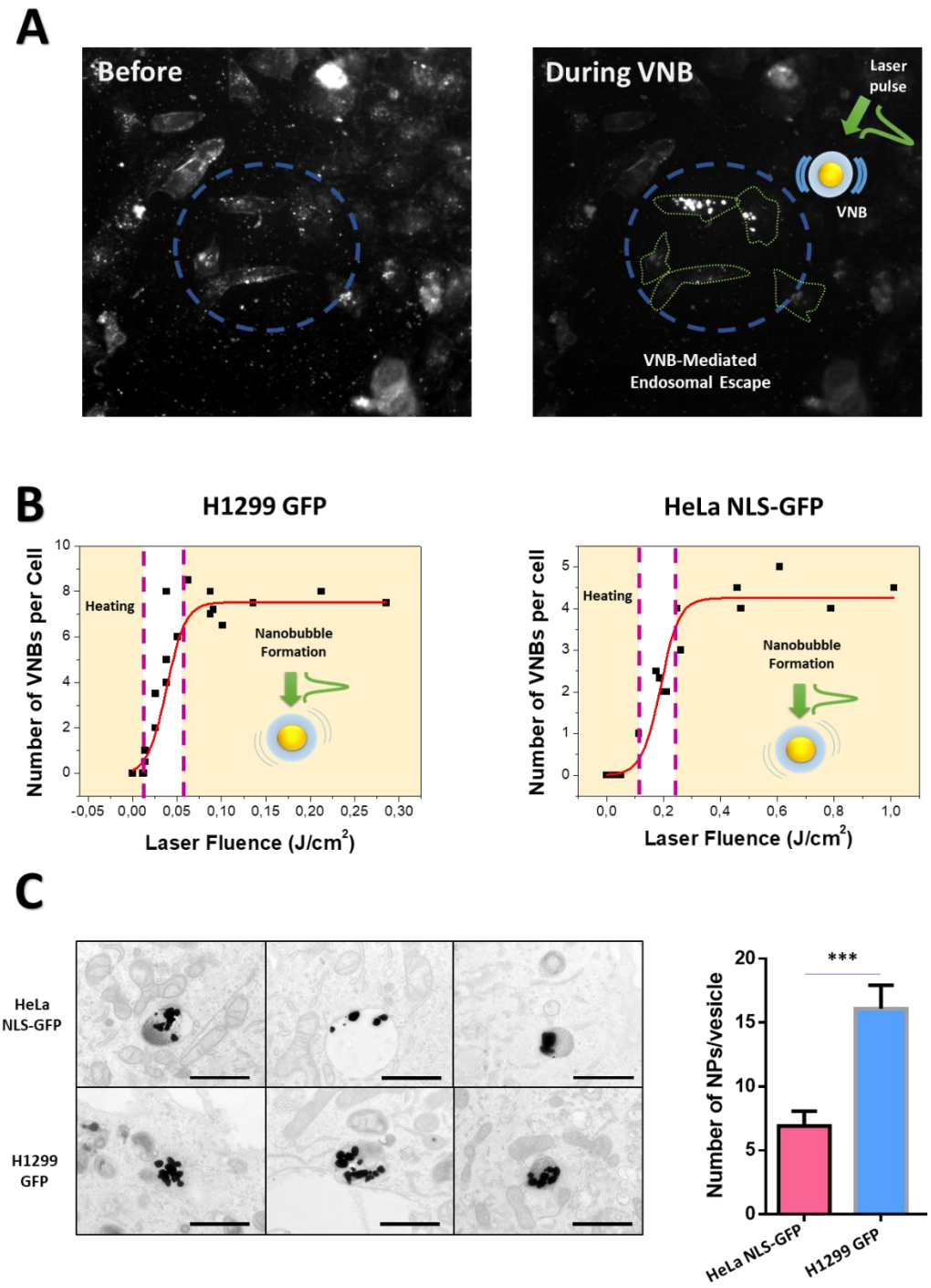

Figure 5. A) Dark field images showing HeLa NLS-GFP cells before and during VNB formation upon irradiation with 1 laser pulse. The irradiation area is indicated by the dashed blue circle while the boundary of the irradiated cells is highlighted by green lines. B) VNB fluence threshold calculated from dark field images for endocytosed AuNP carriers in H1299 GFP (0.061 J/cm²) and HeLa NLS-GFP cells (0.209 J/cm²). The VNB and heating regimes are highlighted in yellow. C) TEM images of H1299 GFP and

HeLa NLS-GFP cells show internalized siRNA/AuNP within endosomes. The average number of NPs per endosome was found to be different in both cell types. The scale bars are 1 μm. Data are represented as mean ± SEM (n = 20 vesicles over 15 cells). Statistical significance was indicated (***$p < 0.001$).

Laser-induced endosomal escape and cell transfections.

Knowing the irradiation conditions for inducing heat or VNB in both cell types, we proceeded to investigate the endosomal escape efficiency for both irradiation regimes. We first sought to get a visual confirmation of endosomal release by making use of AuNP carriers loaded with fluorescently labeled siRNA. After 1h incubation with regular HeLa cells, confocal microscopy images showed a dotted pattern in the red fluorescence channel, characteristic for endocytosed nanocarriers. Upon laser irradiation in the VNB or heating regime, AF647-siRNA was released from the endosomes into the cytoplasm as became apparent from the disappearance of AF647 fluorescence from the vesicles. In case of VNB formation the number of labeled vesicles decreased by a factor 8, while this was only a factor 2 in the case of heating (Figure S6). To demonstrate that the disappearance of the signal is not merely due to photobleaching, control experiments were performed using jetPEI polyplexes loaded with AF647 siRNA (which have no photothermal properties). The jetPEI/AF647-siRNA polyplexes were incubated for 1 h and irradiated with laser pulses at the VNB fluence. As illustrated in Figure S6 B, no significant changes were found after the laser exposure, even when 3 pulses were applied to each location. This indicates that the changes observed in the heating and VNB conditions are due to AF647-siRNA release from the endosomes and not because of mere photobleaching.

Next, we proceeded with unlabeled siRNA targeting GFP to measure knockdown efficiency upon irradiation in the VNB or heating regime. siRNA/AuNP were incubated with H1299 GFP and HeLa NLS-GFP cells for 1h at a concentration of 1.53×10^8 particles/mL. As shown in Figure S7, successful downregulation was achieved for both irradiation conditions in a time-dependent manner. Maximum downregulation in H1299 GFP cells was observed after 24 h, after which GFP expression gradually restored again. This is in line with a previous report on heat-mediated endosomal escape in H1299 GFP

cells using continuous laser irradiation.[11] In HeLa NLS-GFP cells, knockdown was found to increase further to 48 h. Having established the optimal read-out points for both cell types (24 h for H1299 GFO and 48 h for HeLa NLS-GFP), we proceeded with determining the nanocarrier concentration that provides efficient downregulation with acceptable toxicity (Figure S8). Cells were incubated with siRNA/AuNP at increasing concentrations, ranging from 0.15×10^8 to 18.1×10^8 particles/ml, corresponding to an siRNA concentration ranging from 0.2 to 20 nM. GFP fluorescence was again quantified by flow cytometry, while cell metabolic activity (a proxy for viability) was measured in parallel by MTT assay. As can be seen in Figure S8, GFP expression and cell viability gradually decreased in a concentration dependent manner. Based on these results, we selected 1.53×10^8 particles/ml (= 2 nM siRNA) as the most optimal condition to proceed, as it provided clear downregulation with good cell viability >70% for both cell types and irradiation regimes. Note that no significant decrease in the GFP expression was observed for controls without irradiation for both cell types, proving that the laser trigger is required in order to induce endosomal escape and gene silencing.

Having now also established the optimal nanocarrier concentration, we finally performed a direct comparison in transfection efficiency between VNB and heat mediated endosomal escape. As a reference we included siRNA transfections by plasma membrane photoporation[19] and the commonly used RNAiMAX transfection reagent.[28] As can be seen in Figure 6A, at 2 nM siRNA, VNB and heat mediated endosomal escape performed equally well in H1299 GFP cells with ~50% knockdown. Plasma membrane photoporation did not show significant downregulation at 2 nM siRNA as this procedure needs a much higher concentration of siRNA in the cell medium to achieve sufficient influx in the cells by passive diffusion. Indeed, when increasing the siRNA concentration in the cell medium to 1 µM ~60% downregulation was achieved for plasma membrane photoporation as well. RNAiMAX, finally, gave the best result in H1299-GFP cells with ~70% knockdown. When looking at the results for HeLa NLS-GFP cells in Figure 6B, VNB mediated endosomal escape clearly provided the best results with ~55% knockdown. For heat mediated endosomal escape this was markedly less with ~20% knockdown. This was similar to what was obtained with plasma membrane photoporation at 2 nM siRNA. Increasing the

siRNA concentration in the cell medium to 1 µM slightly improved those results to ~30% knockdown, which was virtually the same as what was achieved with RNAiMAX. Together these results show that VNB mediated endosomal escape performed well in both cases, while the success of heat mediated endosomal escape is cell type dependent. This is presumably due to the fact that VNB formation is a fairly drastic nanoscale phenomenon that performs its action as soon as the VNB laser fluence threshold is reached, independent of the number of AuNP present per endosome. Instead, for heat-mediated endosomal escape, the amount of generated heat that leads to pore formation by lipid lateral diffusion and stabilization of defects in the endosomal membrane[29] will logically depend on the number of AuNP present per endosome. Since the number of AuNP per endosome was markedly more in H1299 as compared to HeLa cells, it gives a plausible explanation as to why heat-mediated endosomal escape was less effective in HeLa's.

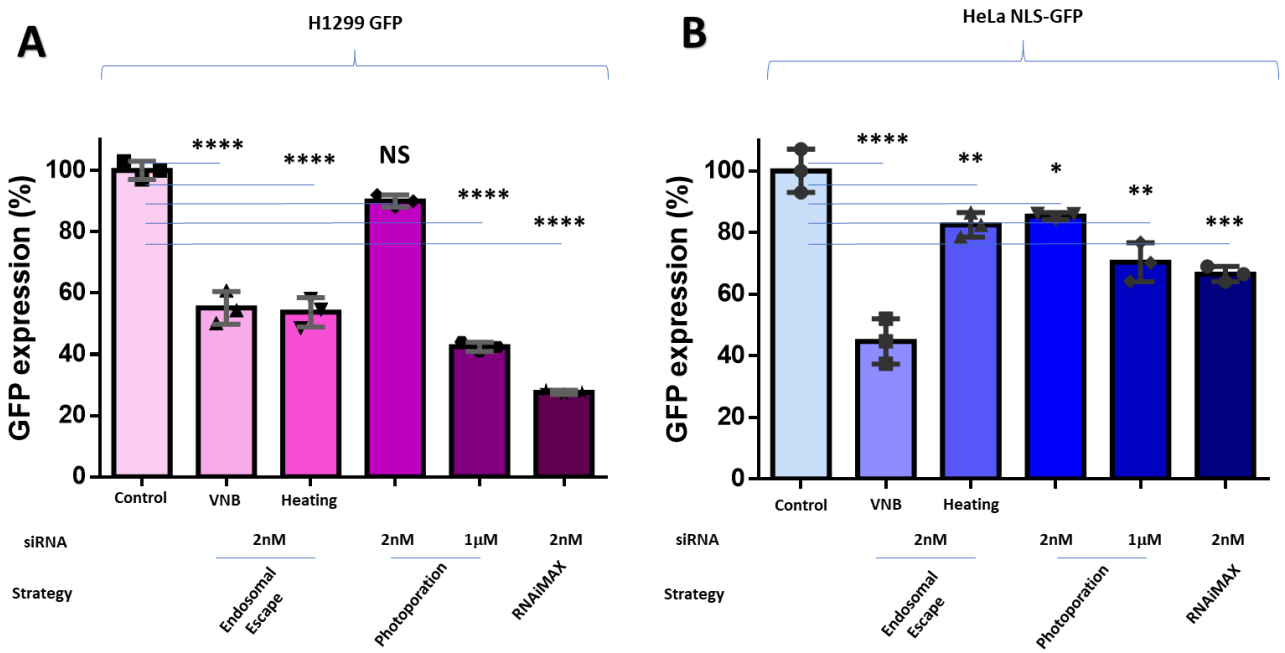

Figure 6. Comparison of VNB- and heat- mediated endosomal escape for siRNA gene silencing. A) GFP expression level after 24 h for different treatments in H1299 GFP cells (pink-purple bars): laser treatment for VNB regime (fluence: 0.08 J/cm^2) and heating regime (fluence: 0.03 J/cm^2) using 2nM

siRNA final concentration; plasma membrane photoporation at 1μM and 2nM siRNA concentrations; lipofection using RNAiMAX lipofectamine at 2nM siRNA final concentration. B) GFP expression level after 48 h for different treatments in HeLa NLS-GFP cells (light-dark blue bars): laser treatment for VNB regime (fluence: 0.229 J/cm^2) and heating regime (fluence: 0.112 J/cm^2) using 2nM siRNA final concentration; plasma membrane photoporation at 1μM and 2nM siRNA concentrations; lipofection using RNAiMAX lipofectamine at 2nM siRNA final concentration. Data are represented as mean ± SEM for 3 independent repeats minimum ($n \geq 3$). Statistical significance, with respect to the untreated cells, is indicated when appropriate (NS = not significant, *$p < 0.05$, **$p < 0.01$, ***$p < 0.001$, ****$P<0.0001$).

Influence of light-triggered endosomal escape regimes on the cell transcriptome

While metabolic assays such as the commonly used MTT assay give information on gross changes in metabolic activity such as acute toxicity, they do not allow unveiling subtle changes in cell homeostasis, or the underlying biological processes that are responsible for cell toxicity. That is why we performed a whole transcriptome analysis at different timepoints after VNB- or heat-mediated endosomal escape in comparison with untreated control cells. We performed this in-depth analysis on HeLa cells incubated with siRNA/AuNP for 1h at a concentration of $1.53x10^8$ NPs/mL (2nM siRNA) and with readout points at 6 h, 24 h and 48 h after laser treatment.

A differential gene expression analysis was performed for two pairs of conditions: VNB-regime versus untreated control, and heating-regime versus untreated control. Genes were defined as significantly down- or upregulated when their levels differed by more than 2 fold ($|\log_2(\text{foldchange})|>1$) and the adjusted p-value was smaller than 0.05 (using Benjamini-Hochberg method for multiple comparisons) (Supplementary Data 1-6). Volcano plots of $\log_2$(fold changes) versus minus the $\log_{10}$ *p*-value were plotted for every timepoint (Figure 7). This revealed that the VNB regime induced a more pronounced effect on the cell's transcriptional activities compared to the heating regime at the earliest (6 h) timepoint,

as can be seen from the higher number of differentially expressed genes (DEGs) (Supplementary Table S1). Remarkably, this initial difference strongly decreased 24 h after treatment, where the number of significant DEGs strongly dropped especially in the VNB regime. 48 h after treatment, the number of significant DEGs increased again in both cases to similar levels. To assess to which extent the cellular response to both treatments differs after laser treatment, we directly compared gene expression in the VNB-regime versus the heating-regime at the three timepoints (6 h, 24 h and 48 h). At the early (6 h) timepoint, 560 genes were found to be significantly differentially expressed (padj<0.05; |log2(foldchange)|>1), which dropped tremendously to only 20 DEGs at 24 h and 1 DEG at 48 h (Supplementary Data 7). This implies that only at early time points after treatment there is a significant difference in the effect of both methods on the cell's transcriptional activities, whereas the cellular response is virtually identical at later timepoints (24 h and 48 h) after treatment.

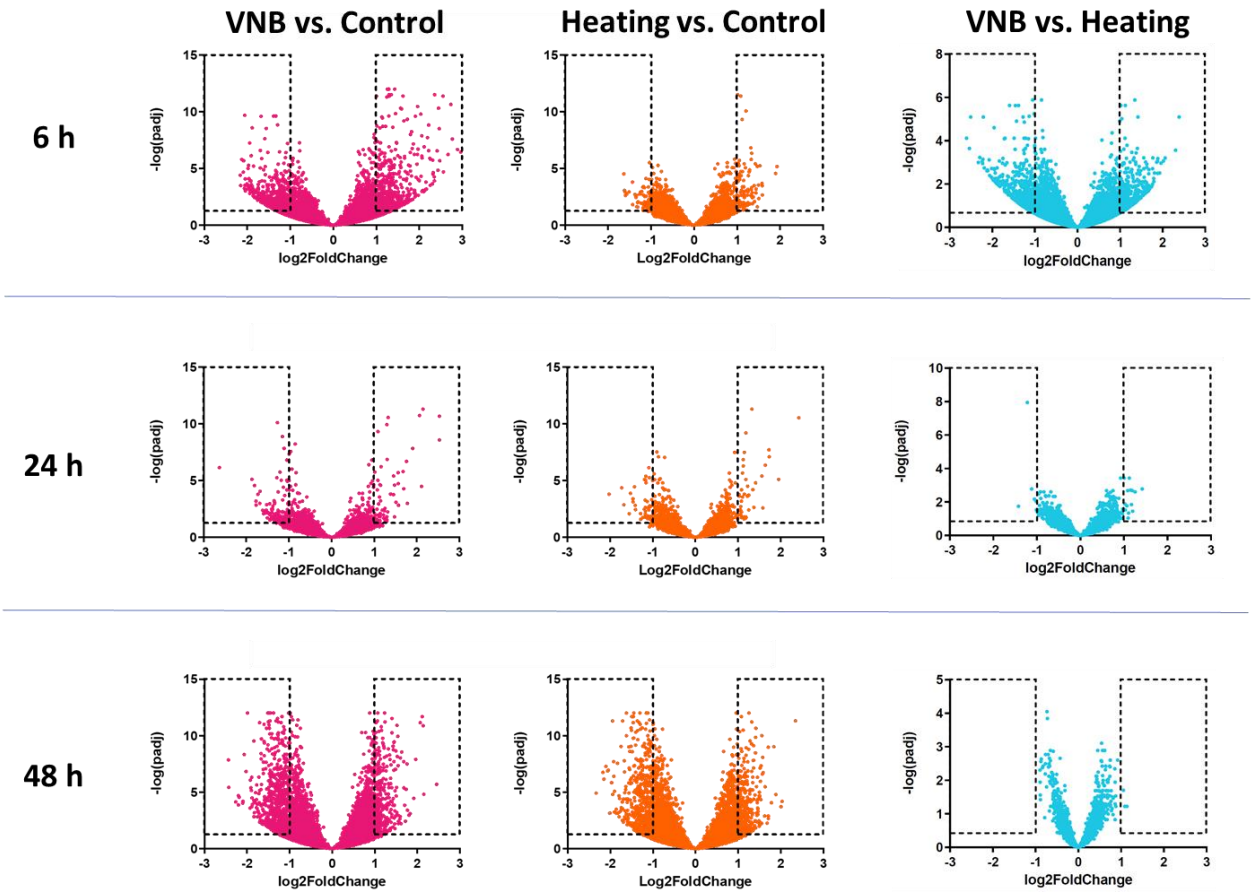

Figure 7. Volcano plots of differential gene expression between cells treated with VNB- or heating-mediated endosomal escape versus untreated (control) cells. For three time points (6 h, 24 h, 48 h) differential gene expression was assessed for both endosomal escape regimes (optimized conditions: $1.53x10^8$ NPs/mL and 2nM siRNA) versus control (pink and orange), and versus each other (cyan). Log2FoldChanges are plotted versus -log(padj), with significantly differentially expressed genes (DEGs: padj<0.05; $|\log_2(\text{foldchange})|>1$) situated in between the dotted marks.

To extract biological knowledge from the large lists of DEGs, we analyzed them further with the Genecodis platform[30–32], which allows to uncover the biological annotations that are statistically overrepresented in the input list. More specifically, we looked at which biological processes from the Gene Ontology (GO) database[33,34] were overrepresented in heating compared to control and in VNB compared to control and this for all three time points (Figure 8). In both treatment regimes, 6 h after laser treatment, various GO categories related to programmed cell death responses were amongst the most significantly represented (e.g. VNB: apoptotic process, GO:0006915; heating: regulation of programmed cell death, GO:00043067). However, at the same time, various GO categories related to cell proliferation were represented as well (e.g. positive regulation of cell proliferation, GO:0008284). 24 h after laser treatment, apoptotic responses were dramatically less represented in both treatments, while GO categories related to cholesterol metabolism were most significantly represented (e.g. cholesterol biosynthetic process, GO0006695). Finally, 48 h after laser treatment, the GO categories of cell division (GO:0051301) and DNA repair (GO:0006281) were most significantly enriched.

Heating 6 h

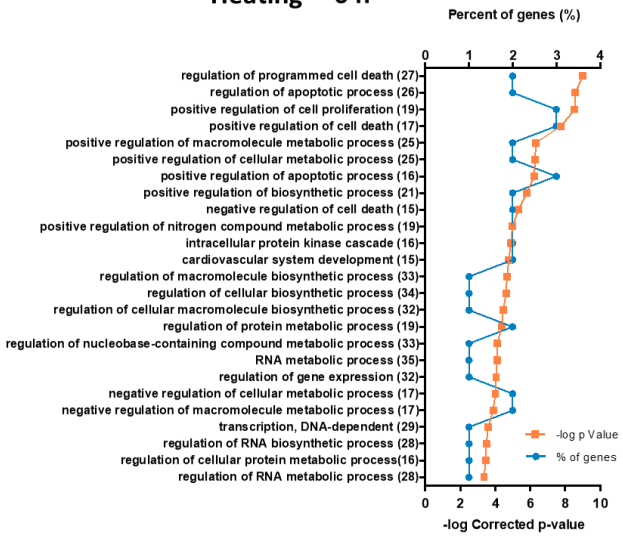

VNB 6 h

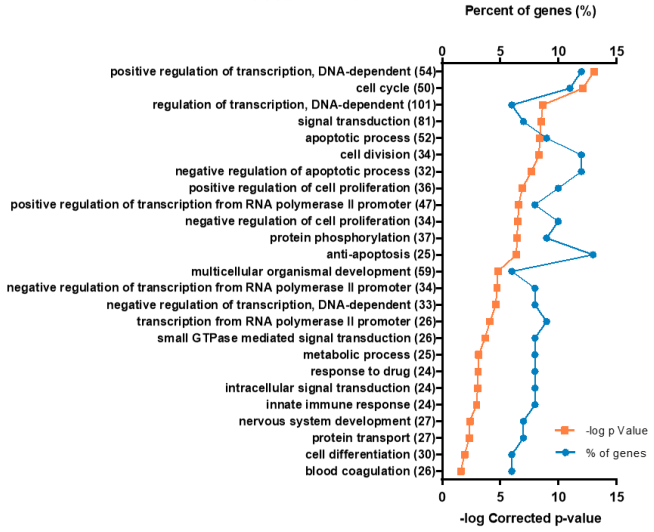

Heating 24 h

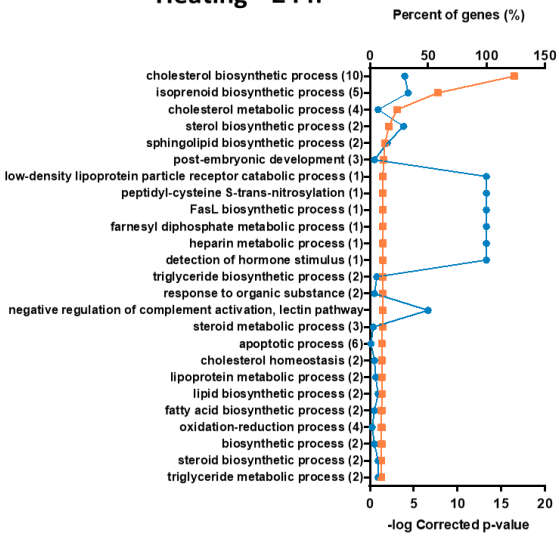

VNB 24 h

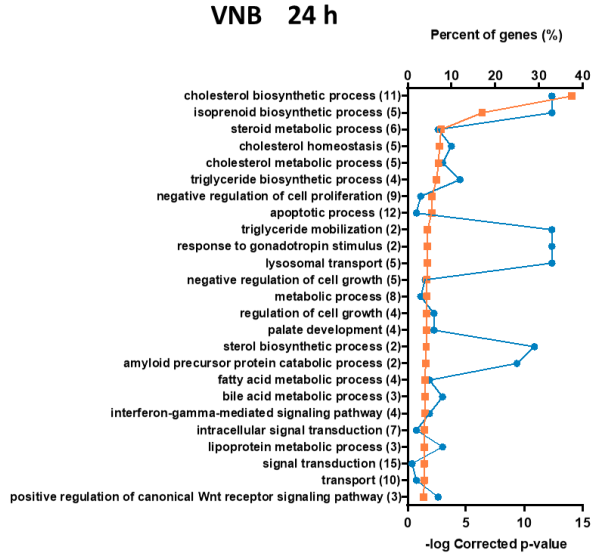

Heating 48 h

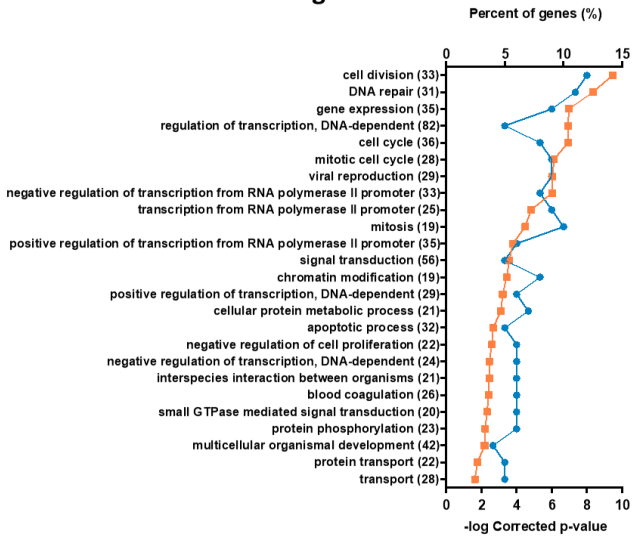

VNB 48 h

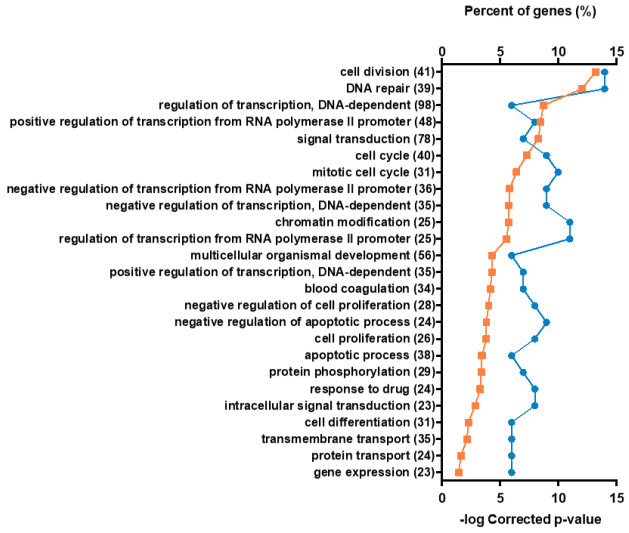

Figure 8. Gene Ontology (GO) enrichment analysis in DEGs between VNB- and heating-mediated regimes versus control. DEGs (p<0.05; $|\log_2(\text{foldchange})|>1$) were fed into the online GeneCodis platform for enrichment analysis of the Biological Process category from the GO database. For every comparison, the -log Corrected p-value (hypergeometric distribution) and the gene percentage is plotted.

The downside of an enrichment analysis method such as GeneCodis is that it only focuses on the number of DEGs observed in a given pathway to decide whether it is significantly dysregulated, while they do not consider the position of the genes (up- or downstream) or how genes interact with each other within a given pathway. Neither is information given on the direction of dysregulation, i.e., whether a certain process is activated or inhibited. Therefore, we additionally used the Signaling Pathway Impact analysis (SPIA) algorithm,[35] implemented in R, to identify pathways that are significantly activated or inhibited (pFDR (false discovery rate) <0.05) compared to the control condition. This was done for the latest time point (48 h) since potential long-term stress-responses are of primary concern from a therapeutic point of view. While GeneCodis analysis showed the DNA repair GO category to be amongst the most significantly enriched biological processes in both treatments, in the SPIA analysis none of the KEGG pathways related to DNA repair ((base excision repair (hsa03410), nucleotide excision repair (hsa03420), homologous recombination (hsa03440) and non-homologous end-joining (hsa03450)) appeared, indicating that when taking all pathway information (gene topology, gene interaction, etc) into account, overall these pathways are not activated nor inhibited compared to the control (Supplementary Tables S2A and B). We additionally checked whether programmed cell death might be significantly activated compared to the control. For both heating and VNB, no programmed cell death pathways (such as apoptosis (hsa24210) and necroptosis (hsa04217)) were found to be significantly affected compared to the control by the SPIA algorithm. To be sure we also checked this for the earlier time points (6 h and 24 h), again finding that apoptosis nor necroptosis were significantly activated or inhibited compared to the control (Supplementary Tables S2C-F). Together this leads us to conclude that the differential expression of genes involved in programmed cell death pathways and in DNA repair pathways as found by

GeneCodis analysis, overall does not result in a significant activation or inhibition of these pathways at any of the time points when taking into account pathway information such as gene topology and gene interaction.

DISCUSSION

AuNP and cargo integrity upon ns pulsed laser irradiation.

The photothermal properties of AuNPs has sparked interest in recent years to explore them as light responsive drug delivery systems, in particular as a very promising strategy for overcoming the endosomal barrier. Even though some promising reports have appeared using a variety of laser irradiation regimes, it remains unknown at present which photothermal mechanism is to be preferred in terms of cargo release, endosomal escape, transfection efficiency or long-term effects on cell homeostasis. Two photothermal effects are of major importance. The most common one is straightforward heat generation, as if often accomplished with readily available continuous wave lasers. However, using nanosecond pulsed lasers, it has been amply demonstrated that apart from heat it is also possible to induce mechanical stress (with negligible heat transfer) if AuNP are irradiated above the laser fluence threshold for vapor nanobubble generation. In this study, therefore, we aimed to perform an in-depth comparative study between light-induced endosomal escape through heat or VNB-formation using nanosecond pulsed laser light. To this end, we designed an AuNP-based nanocarrier that could be efficiently loaded with siRNA (siRNA/AuNP). The first question that we explored was related to the integrity of the cargo and of the carrier itself after laser irradiation.[22] As it is known that size reduction of AuNP can occur upon laser irradiation by either photothermal surface evaporation or Coulomb explosion mechanisms,[24,36] it came as no surprise that TEM images showed a size reduction of the AuNP core upon irradiation for both regimes (Figure 2 C and D), with the smallest fragments being formed for the case of VNB formation. The question then comes to which extent particle fragmentation might affect the release and integrity of the siRNA cargo itself. As confirmed by two independent measurement techniques (agarose gel electrophoresis, and µGel electrophoresis), siRNA was released intact and equally efficient from the carriers for both

irradiation conditions (Figure 3). This was further corroborated by the transfection experiments in which the released siRNA was able to downregulate GFP expression in two different cell types.

Cell type dependency of the laser fluence.

An important finding that emerged from our experiments is that the laser fluence levels to generate heat or VNB after carrier endocytosis differs substantially from those in a colloidal dispersion and strongly depends on the cell type as well. We could explain this observation by the fact that particles are clustered inside the vesicles along the endocytic pathway in a cell-dependent manner. It has been reported that clustering of AuNPs can lead to a considerable decrease in the VNB threshold.[27] The lowest VNB threshold value was found for H1299 GFP cells, which had the highest number of particles per vesicle (~ 17 NPs/vesicle) as determined from TEM analysis. HeLa's on the other hand only had ~7 NPs/vesicle, leading to a substantially higher laser irradiation threshold. These observations clearly show that the clustering degree plays a critical role on the effective laser fluence values that are needed to generate distinct photothermal phenomena in cells.

VNB- and heat-mediated endosomal escape and cell transfections.

While VNB-mediated cell transfections were equally efficient in both cell types (50 % knockdown), this was not the case for the heating regime which produced substantially less downregulation (~20%) in HeLa NLS-GFP cells (Figure 6 and Figure S8). We hypothesize that this is due to the fact that VNB-induced endosomal escape works independently of the number of AuNPs per endosome. As soon as the VNB laser fluence threshold is reached, VNBs emerge whose strong physical force will rupture the endosomal membrane. On the other hand, heat destabilization of the endosomal membrane depends the amount of heat that is generated, which in turn depends on the number of AuNPs inside a particular endosome. In connection to the TEM observations, HeLa NLS-GFP cells showed a substantially lower number of particles inside the vesicles, which will lead to less heat generation and reduced siRNA release from the endosomes than in the case of H1299 GFP cells. Together we conclude

that the mechanical forces by VNB produce a more consistent endosomal escape and transfection efficiency independent of cell type instead of heat-mediated endosomal escape. In addition, the downregulation levels after VNB-mediated endosomal escape were compared with AuNP-mediated cell membrane photoporation, giving similar gene silencing results but at a 500-fold reduced siRNA concentration for the siRNA/AuNP carriers. Thus, the approach represents a significant improvement over physical transfection methods that are based on the permeabilization of the plasma membrane in which case a very high concentration of cargo molecules is needed (typically micromolar range) to drive molecules into the cytoplasm by passive diffusion.[19]

Influence of light-triggered endosomal escape on cell homeostasis

Rather than monitoring only acute cytotoxicity as is traditionally done in transfection studies, we here performed a detailed whole transcriptome analysis at different time points to investigate potential short and long(er) term effects on cell homeostasis. Based on the number of DEGs, at the earliest time point (6 h) a stronger cellular response was seen to the VNB-regime compared to the heating regime. Responses to both treatments, however, strongly converged at the latest time point (48 h) as was seen from the absence of DEGs when comparing both regimes directly. Enrichment analysis of GO biological processes in the DEGs mostly revealed differences between the time points for the same treatment, rather than differences between both treatments at a certain time point.

Importantly, pathway analysis using SPIA showed no programmed cell death pathways (such as apoptosis (hsa24210) and necroptosis (hsa04217)) to be significantly altered (activated or inhibited) for either of both laser treatment regimes compared to untreated control cells. In addition, even though it has been previously reported that tiny gold fragments (particles of ~2 nm) inside the cell can intercalate into the genomic DNA and induce genotoxicity,[37,38] the absence of DNA repair pathways in the pathway analysis at all three time points, indicated that possible DNA damage due to small AuNP fragments is absent. These results, in combination with the transfection performance, position VNB-mediated

endosomal escape as a safe and realistic strategy for controlled drug delivery that can generate consistent knockdown efficiencies for different cell types.

CONCLUSIONS

In summary, using siRNA/AuNP plasmonic nanocarriers we have performed a rigorous evaluation of two distinct photothermal phenomena - heating and VNB formation – for inducing endosomal escape and gene silencing with minimal effects on cell homeostasis. Contrary to heat-mediated endosomal escape, VNB generation produced excellent transfection levels independent of the cell type. Since neither of both photothermal phenomena induced long-term changes in cell homeostasis, these results position VNB-mediated endosomal escape as the more consistent mechanism for light-induced transfections with plasmonic nanocarriers. An important caveat, however, is that the laser fluence for VNB generation turned out to be cell-type dependent, necessitating optimization of laser irradiation conditions per application.

MATERIALS AND METHODS

Materials.

The following materials were used as obtained: $HAuCl_4$ (Acros Organics); Sodium Citrate (Aldrich); Sodium L-Ascorbate (Sigma-Aldrich); Hyaluronic acid 20 kDa (HA) (Aldrich); Poly(diallyldimethylammonium chloride) solution 20 wt. % in H_2O (PDDAC) (Aldrich). DMEM/F-12, Opti-MEM, L-Glutamine, Penicillin/Streptomycin solution (5000 IU/mL penicillin and 5000 μg/mL streptomycin) (P/S), Fetal Bovine Serum (FBS), Trypan Blue, 0.25% Trypsin-EDTA, and Dulbecco's phosphate-buffered saline 1× without $Ca^{2+/}Mg^{2+}$ (DPBS-) were supplied by GibcoBRL (Merelbeke, Belgium). Hoechst 33342 was purchased from Molecular Probes (Erembodegem, Belgium). Lipofectamine RNAiMAX reagent was purchased from Invitrogen. Twenty-one-nucleotide siRNA duplexes targeting the enhanced green fluorescent protein (siEGFP) and negative control duplexes (siCTRL) were purchased from Eurogentec (Seraing, Belgium). siEGFP: sense strand = 5'-CAAGCUGACCCUGAAGUUC**tt**-3'; antisense strand = 5'-GAACUUCAGGGUCAGCUUG**tt**-3'.

siCTRL: sense strand = 5'-UGCGCUACGAUCGACGAUG**tt**-3'; antisense strand = 5'-CAUCGUCGAUCGUAGCGCA**tt**-3' (lower case bold letters represent 2'-deoxyribonucleotides, capital letters are ribonucleotides). For fluorescence experiments, the siCTRL duplex was labeled with Alexa Fluor 647 dye at the 5' end of the sense strand (Eurogentec).

Au Nanoparticles Synthesis.

The synthesis of AuNPs was performed using the Turkevich method, which is based on the reduction properties of boiling citrate solutions.[20] Briefly, Au nanoparticle seeds were produced by reducing a 150 mL 0.2 mM chloroauric acid solution ($HAuCl_4$) with the addition of 0.5 mL of a 0.01 M citrate solution (corresponding to a 1:1 Au/Citrate molar ratio) under heat and rapid stirring for 30 min. These seeds were overgrown to the desired size by addition of Au^{3+} and ascorbate solutions in equimolar concentrations (0.01 M) through capillary tubes and controlling the maximum in the Extinction spectrum by UV-vis. When the dipolar LSPR peak matched the LSPR peak of the desired size (i.e., between 560-570 nm for NPs with 90-100 nm in diameter) the synthesis was stopped.

The morphological characterization of the AuNPs was performed combining UV-vis spectroscopy, TEM, dynamic light scattering (DLS), and electrodynamic modeling using Mie theory. The overall results after combining all of these different techniques and modeling indicate that the average diameter of Au NPs was 95 nm with a typical concentration of $6.4x10^8$ NPs/mL, estimated using the experimental extinction intensities at the maximum wavelength (λ_{max} = 564 nm), and the cross section calculated using Mie theory ($\sigma_{ext(568\ nm)}$ = 5.2 x 10^{-10} cm²/NP) for spherical particles with the suitable diameter (determined by TEM).

Au NP Surface Functionalization.

The synthetized NPs were further functionalized following a polyelectrolyte strategy. First, NPs were functionalized with 20kDa hyaluronic acid (HA) at a final concentration of 0.02 mg/mL. After reaction overnight, the HA-NPs were washed by centrifugation (5 min at 5000 rcf) and resuspended in ddi water (zeta potential ~ -40 mV). Next, the HA-NPs were further functionalized by adding poly(diallyldimethylammonium chloride) solution 20 wt. % in H_2O (PDDAC) at a final concentration of

0.06 mg/mL and allowed to react for at least 2 hours. After this time the PDDAC-HA-NPs were washed by centrifugation (5 min at 5000 rcf) and stored for further experiments.

Functionalization with siRNA was performed on the same day of the experiment by direct incubation for at least 1 hour of PDDAC-HA-NPs with optimized amounts of siRNA according to complexation experiments performed with gel electrophoresis (1% agarose) and zeta potential measurements.

Knockdown Experiments.

H1299 expressing green fluorescence protein (GFP) cells (H1299 GFP, lung epithelial cells derived from metastatic lymph nodes, ATCC-CCL 5803)[25] were cultured in Roswell Park Memorial Institute (RPMI) 1640 medium supplemented with 10% FBS, 2 mM L-Glutamine and 100 µg/mL P/S. HeLa (cervical adenocarcinoma cells, ATCC CCL-2) and stably transfected HeLa cells with nuclear-localized signaling expressing GFP (HeLa NLS-GFP)[26] were cultured in Dulbecco's modified Eagle's medium supplemented with growth factor F12 (DMEM/F-12) supplemented with 10% FBS, 2 mM L-Glutamine, and 100 µg/mL P/S. Cells were incubated at 37 °C in a humidified atmosphere containing 5% CO2. Cellular experiments were performed on cells with a passage number below 25.

Before incubation with the NPs and the laser treatment, cells (15000 cells/well) were cultured in 96 well plates (#92096, TPP, Switzerland) for 24 h before treatment. Prior the laser treatment, the cells were incubated with the siRNA-functionalized Au NPs for 1 hour in Opti-MEM at concentrations indicated in the text, followed by a washing step to remove any remaining free AuNPs in solution using PBS 1x. After the laser treatment, the cells were washed and supplied with fresh cell medium. Images of the prepared cell samples were taken by confocal microscope (C1-si, Nikon, Japan) to quantify the loading efficiency (number of stained vesicles). The samples were also prepared for measurement by flow cytometry. The cells were washed with PBS 1x, detached by incubation with trypsin/EDTA 0.25%, and diluted with complete cell culture medium. Following centrifugation (5 min, 300g), the cell pellet was resuspended in flow buffer (PBS supplemented with 1% BSA and 0.1% sodium azide), and placed on ice until flow cytometric analysis. Fluorescence was measured on aminimum of 15000 events per sample

(488 nm excitation with argon laser and detection with a 530/30 nm bandpass filter) by flow cytometry using a CytoFLEX (Beckman Coulter, Krefeld, Germany) flow cytometer. FlowJo software (Treestar Inc., Ashland, USA) was used for analysis. For calculating the percentage of EGFP expression after siRNA gene silencing efficiency, EGFP signal intensity was quantified as the mean fluorescence intensity (MFI) of cells treated with siEGFP divided by the average intensity of cells treated with a non-targeting control siRNA (siCTRL) under identical experimental conditions according to the following equation: EGFP (%) = [(MFI siEGFP) / (MFI siCTRL)] x 100% with MFI siEGFP indicating the mean fluorescence intensity of cells incubated with anti-EGFP siRNA and MFI siCTRL indicating the mean fluorescence intensity of cells incubated with negative control siRNA.

Cytotoxicity Studies.

For metabolic activity measurements, the AuNPs were functionalized with siCTRL. A typical experiment consisted in seeding 15000 cells in 96-well plates 1 day in advance. After incubation of the NPs for 1 hour, the cells were washed and the laser treatment was performed. Next, cells were washed and new medium was added. The cells were incubated for 3 h before addition of 3-(4,5-dimethyl-2-thiazolyl)-2,5-diphenyl-2H-tetrazolium bromide (MTT) solution (1 mg/mL in DPBS). After 3 h, the solution was removed, and the newly formed purple formazan crystals were dissolved by addition of DMSO. The plates were covered in aluminum foil and placed on an orbital shaker (Rotamax 120, Heidolph, Germany) for 45 min at 120 rpm. As negative control, a blank sample with medium was used, while as a positive control untreated cells were used. UV absorbance was measured on a plate reader (Wallac Envision, Finland) at 590 nm (metabolic activity) and 690 nm (reference wavelength).

Irradiation Setup.

The generation of Au NPs heating and VNB formation were performed using a homemade setup including an optical system and an electric timing system, as reported before.[19] Briefly, the setup consists in a pulsed laser with a (pulse duration of ~7 ns, pulse repetition rate of 20 Hz) tuned at a wavelength of 561 nm (Opolette HE 355 LD, OPOTEK Inc., CA, USA) and used for irradiation of the Au NPs.

The setup has the possibility to be used for detection of VNB formation using a dark-field condenser, as VNBs can be very well detected by dark-field microscopy due to their scattering efficiency. The detection was achieved by synchronizing the camera (EMCCD camera, Cascade II: 512, Photometrics, Tucson, AZ, USA) with the pulsed laser by an electronic pulse generator (BNC575, Berkeley Nucleonics Corporation, CA, USA). The laser pulse energy was monitored by an energy meter (J-25MB-HE&LE, Energy Max-USB/RS sensors, Coherent) synchronized with the pulsed laser. The laser fluence was calculated as the average energy of a single laser pulse divided by the laser beam area (150 μm diameter).

For laser treatments, a 96-well plate was positioned onto an electronic translation table (H117, Prior, UK) was used to scan the laser beam line by line across the entire sample. The scanning speed was 22 mm/s, and the distance between subsequent lines was 0.15 mm (diameter of the laser beam). This way each location in the sample receives a single laser pulse, with a total treatment time of ~3.4 min per well.

VNB threshold measurements.

Colloidal dispersion of 1.8×10^9 NPs/mL of AuNP in water were prepared to detect VNB of isolated NPs. To detect VNB on cells, 150000 cells were seeded in 50 mm glass bottom dish (MatTek Corporation, US) two days in advance. Cells were incubated with different concentration of AuNP in Opti-MEM for 1 hour. Unbound particles were washed with DPBS after which fresh cell culture medium was added. The isolated NPs or the cells containing the uptake NPs were exposed to 1 laser pulse while the camera took an image before and during the laser pulse. At the same time, the pulse intensity was recorded by an energy meter. The number of VNB was counted in each image resulting in graph that expresses the number of VNB as function of the laser fluence. The graphs were fitted with a Boltzmann sigmoid function allowing to determine the VNB threshold as the 90% of probability of generate VNBs according to the fitting.

Integrity of NPs and siRNA cargo after laser pulse.

The laser pulse effect on the siRNA-functionalized Au NPs was evaluated for the two different regimes (heating and VNB formation). A typical experiment consisted in functionalizing PDDAC/NPs

with siCTRL by direct mixing and incubation for at least 1 hour. After this period the particles were centrifuged and resuspended in PBS, and placed onto a glass slide previously modified with a plastic container with a width matching the focal plane of the optical system of the irradiation setup, which was further sealed with a coverslip. After laser irradiation the samples were collected for further characterization.

For characterization of the NPs integrity, the collected samples were seeded onto a TEM grid for electron microscopy imaging or placed in a cuvette for UV-vis measurements.

The possible degradation of the cargo was evaluated by μ-gel electrophoresis for sizing and quantification of the siRNA fragmentation using an Agilent chip.

Extinction Measurements.

The characterization by UV-Vis spectroscopy was performed using a NanoDrop 2000c Spectrophotometer (Thermo SCIENTIFIC), scanning in the 250-850 nm range with a 1 cm cuvette at room temperature.

DLS Measurements.

The characterization by dynamic light scattering (DLS) was performed after being transferred to disposable folded capillary cells (Malvern, Worcestershire, UK) to determine hydrodynamic diameter, polydispersity index, and ζ potential via the NanoZS Zetasizer (Malvern Instruments, Hoeilaart, Belgium).

Transmission Electron Microscopy.

Transmission electron microscopy (TEM) images were obtained at the VIB-UGent Transmission Electron Microscopy-Core facility using a JEM 1400plus transmission electron microscope (JEOL, Tokyo, Japan) operating at 80 kV.

Nanoparticle samples were prepared by adding one drop (~ 50 μL) of the colloidal dispersion onto formvar/C-coated hexagonal copper grids (EMS G200H-Cu) for 20 min and washed 5 times in double distilled H_2O.

For imaging of cells sections, HeLa NLS-GFP cells and H1299 GFP cells were grown on glass coverslips and fixed in 4% paraformaldehyde and 2.5% glutaraldehyde in 0.1 M NaCacodylate buffer (pH

= 7.2) for 4 hours at room temperature, followed by fixation overnight at 4℃. After washing three times for 20 min with buffer solution, cells were post fixed in 1% OsO4 with 1.5% K3Fe(CN)6 in 0.1 M NaCacodylate buffer at room temperature for 1 hour. After washing in ddH_2O, cells were subsequently dehydrated through a graded ethanol series, including a bulk staining with 1% uranyl acetate at the 50% ethanol step followed by embedding in Spurr's resin. Ultrathin sections of a gold interference color were cut using an ultra-microtome (Leica EM UC7), followed by a post-staining in a Leica EM AC20 for 40 min in uranyl acetate at 20 °C and for 10 min in lead stain at 20 °C. Sections were collected on formvar-coated copper slot grids.

Whole Transcriptome Analysis.

For the whole transcriptome analysis the AuNPs were functionalized with siCTRL at a final concentration of 2nM. A typical experiment consisted in seeding 15000 cells in 96-well plates 1 day in advance. After each treatment (cell control, VNB or Heating) the cells were washed and stored at 37 °C until the specific time point in which they were lysed for further analysis. The selected time points were 6, 24 and 48 hours after the treatment. Before lysis, cells were washed with 125µL of PBS 1x at room temperature, followed by 10 min incubation with the lysis mixture (SingleShot™ Cell Lysis Kit, Bio-Rad). Lysed cells were transferred to a 384-well PCR plate for thermal cycle (5 min at 37°C followed by 5 min at 75°C), after which they were stored at -20°C until the analysis. RNA-sequencing libraries were prepared directly from cell lysates using the Quantseq procedure (Lexogen) according to the manufacturer's instructions. Libraries were quantified by qPCR, equimolarly pooled, and sequenced on a NextSeq500 (Illumina). Reads were mapped to the human genome using Tophat and gene expression counts were generated using HTSeq. Normalization and differential gene expression analysis were performed using DESeq2.

Computational Methods.

The optical response of Au NPs were computed using the Generalized Multiparticle Mie Theory (GMM) as described elsewhere.[39] In all the calculations presented in this work the dielectric function tabulated by Palik for Au was employed.[40]

Statistical Analysis.

All statistical analyses were performed using GraphPad software (La Jolla, CA, USA). One-way ANOVA combined with the post-hoc Dunnett test was applied to compare multiple conditions, whereas the student t-test was used for direct comparison of 2 conditions. Differences with a p-value < 0.05 were considered significant.

ACKNOWLEDGMENT

This research was funded by European Research Council (ERC) under the European Union's Horizon 2020 research and innovation program (grant agreement [648214]). J.L. gratefully acknowledges the financial support from the China Scholarship Council (CSC) (201506750012) and the Special Research Fund from Ghent University (01SC1416). W.H.DV. gratefully acknowledges The Flemish Research Foundation (FWO grant 1152918N, G005819N, 1516619N).

SUPPORTING INFORMATION AVAILABLE

Eight additional figures and two additional table.

REFERENCES

(1) Kanasty, R.; Dorkin, J. R.; Vegas, A.; Anderson, D. Delivery Materials for SiRNA Therapeutics. *Nat. Mater.* **2013**, *12* (11), 967–977.

(2) Pack, D. W.; Hoffman, A. S.; Pun, S.; Stayton, P. S. Design and Development of Polymers for Gene Delivery. *Nat. Rev. Drug Discov.* **2005**, *4* (7), 581–593.

(3) Zhao, L.; Seth, A.; Wibowo, N.; Zhao, C. X.; Mitter, N.; Yu, C.; Middelberg, A. P. J. Nanoparticle Vaccines. *Vaccine* **2014**, *32* (3), 327–337.

(4) Torchilin, V. Intracellular Delivery of Protein and Peptide Therapeutics. *Drug Discov. Today Technol.* **2009**, *5* (2–3).

(5) Selby, L. I.; Cortez-Jugo, C. M.; Such, G. K.; Johnston, A. P. R. Nanoescapology: Progress toward Understanding the Endosomal Escape of Polymeric Nanoparticles. *Wiley Interdiscip. Rev. Nanomedicine Nanobiotechnology* **2017**, *9* (5).

(6) Martens, T. F.; Remaut, K.; Demeester, J.; De Smedt, S. C.; Braeckmans, K. Intracellular Delivery of Nanomaterials: How to Catch Endosomal Escape in the Act. *Nano Today* **2014**, *9* (3), 344–364.

(7) Vermeulen, L. M. P.; Brans, T.; Samal, S. K.; Dubruel, P.; Demeester, J.; De Smedt, S. C.; Remaut, K.; Braeckmans, K. Endosomal Size and Membrane Leakiness Influence Proton Sponge-Based Rupture of Endosomal Vesicles. *ACS Nano* **2018**, *12* (3), 2332–2345.

(8) Meacham, J. M.; Durvasula, K.; Degertekin, F. L.; Fedorov, A. G. Physical Methods for Intracellular Delivery: Practical Aspects from Laboratory Use to Industrial-Scale Processing. *J. Lab. Autom.* **2014**, *19* (1), 1–18.

(9) Qin, G.; Li, Z.; Xia, R.; Li, F.; O'Neill, B. E.; Goodwin, J. T.; Khant, H. A.; Chiu, W.; Li, K. C. Partially Polymerized Liposomes: Stable against Leakage yet Capable of Instantaneous Release for Remote Controlled Drug Delivery. *Nanotechnology* **2011**, *22* (15).

(10) Anderson, L. J. E.; Hansen, E.; Lukianova-Hleb, E. Y.; Hafner, J. H.; Lapotko, D. O. Optically Guided Controlled Release from Liposomes with Tunable Plasmonic Nanobubbles. *J. Control. Release* **2010**, *144* (2), 151–158.

(11) Huschka, R.; Barhoumi, A.; Liu, Q.; Roth, J. A.; Ji, L.; Halas, N. J. Gene Silencing by Gold Nanoshell-Mediated Delivery and Laser-Triggered Release of Antisense Oligonucleotide and SiRNA. *ACS Nano* **2012**, *6* (9), 7681–7691.

(12) Silencing, L. G.; Braun, G. B.; Pallaoro, A.; Wu, G.; Missirlis, D.; Zasadzinski, J. A.; Tirrell, M.; Reich, N. O. Laser-Activated Gene Silencing. *ACS Nano* **2009**, *3* (7), 2007–2015.

(13) Huang, X.; Pallaoro, A.; Braun, G. B.; Morales, D. P.; Ogunyankin, M. O.; Zasadzinski, J.; Reich, N. O. Modular Plasmonic Nanocarriers for Efficient and Targeted Delivery of Cancer-Therapeutic SiRNA. *Nano Lett.* **2014**, *14* (4), 2046–2051.

(14) Patino, T.; Mahajan, U.; Palankar, R.; Medvedev, N.; Walowski, J.; Münzenberg, M.; Mayerle, J.; Delcea, M. Multifunctional Gold Nanorods for Selective Plasmonic Photothermal Therapy in Pancreatic Cancer Cells Using Ultra-Short Pulse near-Infrared Laser Irradiation. *Nanoscale* **2015**, *7* (12), 5328–5337.

(15) Shao, J.; Griffin, R. J.; Galanzha, E. I.; Kim, J. W.; Koonce, N.; Webber, J.; Mustafa, T.; Biris, A. S.; Nedosekin, D. A.; Zharov, V. P. Photothermal Nanodrugs: Potential of TNF-Gold Nanospheres for Cancer Theranostics. *Sci. Rep.* **2013**, *3*, 1–9.

(16) Fraire, J. C.; Coronado, E. A. Design of Plasmonic Probes through Bioconjugation and Their Applications in Biomedicine: From Cellular Imaging to Cancer Therapy. In *Nanobiomaterials in Medical Imaging*; Elsevier Inc., 2016; pp 131–162.

(17) Metwally, K.; Mensah, S.; Baffou, G. Fluence Threshold for Photothermal Bubble Generation Using Plasmonic Nanoparticles. *J. Phys. Chem. C* **2015**, *119* (51), 28586–28596.

(18) Lapotko, D. Optical Excitation and Detection of Vapor Bubbles around Plasmonic Nanoparticles. *Opt. Express* **2009**, *17* (4), 2538.

(19) Xiong, R.; Raemdonck, K.; Peynshaert, K.; Lentacker, I.; De Cock, I.; Demeester, J.; De Smedt, S. C.; Skirtach, A. G.; Braeckmans, K. Comparison of Gold Nanoparticle Mediated Photoporation: Vapor Nanobubbles Outperform Direct Heating for Delivering Macromolecules in Live Cells. *ACS Nano* **2014**, *8* (6), 6288–6296.

(20) Turkevich, John; Cooper, P. H. J. A Study of the Nucleation and Growth Process in the Synthesis of Colloidal Gold. *Discuss. Faraday Soc.* **1951**, *55* (c), 55–75.

(21) Qiu, Y.; Liu, Y.; Wang, L.; Xu, L.; Bai, R.; Ji, Y.; Wu, X.; Zhao, Y.; Li, Y.; Chen, C. Surface Chemistry and Aspect Ratio Mediated Cellular Uptake of Au Nanorods. *Biomaterials* **2010**, *31* (30), 7606–7619.

(22) Liz-marza, L. M. Reshaping, Fragmentation, and Assembly of Gold Nanoparticles Assisted by Pulse Lasers. *Acc. Chem. Res.* **2016**, *49*, 678−686.

(23) Matsuo, N.; Muto, H.; Miyajima, K.; Mafuné, F. Single Laser Pulse Induced Aggregation of Gold Nanoparticles. *Phys. Chem. Chem. Phys.* **2007**, *9* (45), 6027–6031.

(24) Hashimoto, S.; Werner, D.; Uwada, T. Studies on the Interaction of Pulsed Lasers with Plasmonic Gold Nanoparticles toward Light Manipulation, Heat Management, and Nanofabrication. *J. Photochem. Photobiol. C Photochem. Rev.* **2012**, *13* (1), 28–54.

(25) Merckx, P.; Backer, L. De; Hoecke, L. Van; Guagliardo, R.; Echaide, M.; Baatsen, P.; Olmeda, B.; Saelens, X.; Pérez-gil, J.; Smedt, S. C. De; et al. Surfactant Protein B (SP-B) Enhances the Cellular SiRNA Delivery of Proteolipid Coated Nanogels for Inhalation Therapy. *Acta Biomater.* **2018**, *78*, 236–246.

(26) Houthaeve, G.; Xiong, R.; Robijns, J.; Luyckx, B.; Beulque, Y.; Brans, T.; Campsteijn, C.; Samal, S. K.; Stremersch, S.; Smedt, S. C. De; et al. Targeted Perturbation of Nuclear Envelope Integrity with Vapor Nanobubble-Mediated Photoporation. *ACS Nano* **2018**, *12*, 7791−7802.

(27) Lukianova-Hleb, E. Y.; Belyanin, A.; Kashinath, S.; Wu, X.; Lapotko, D. O. Plasmonic Nanobubble-Enhanced Endosomal Escape Processes for Selective and Guided Intracellular Delivery of Chemotherapy to Drug-Resistant Cancer Cells. *Biomaterials* **2012**, *33* (6), 1821–1826.

(28) Morgan, R. G.; Chamber, A. C.; Williams, A. C. Optimized Delivery of SiRNA into 3D Tumor Spheroid Cultures in Situ. *Sci. Rep.* **2018**, 1–10.

(29) Stewart, M. P.; Langer, R.; Jensen, K. F. Intracellular Delivery by Membrane Disruption: Mechanisms, Strategies, and Concepts. *Chem. Rev.* **2018**, *118*, acs.chemrev.7b00678.

(30) Nogales-cadenas, R.; Carmona-saez, P.; Vazquez, M.; Vicente, C.; Yang, X.; Tirado, F.; Marı, J. GeneCodis : Interpreting Gene Lists through Enrichment Analysis and Integration of Diverse Biological Information. *Nucleic Acids Res.* **2009**, *37* (May), 317–322.

(31) Tabas-madrid, D.; Nogales-cadenas, R.; Pascual-montano, A. GeneCodis3 : A Non-Redundant and Modular Enrichment Analysis Tool for Functional Genomics. *Nucleic Acids Res.* **2012**, *40* (May), 478–483.

(32) Carmona-saez, P.; Chagoyen, M.; Tirado, F.; Carazo, J. M.; Pascual-montano, A. GENECODIS : A Web-Based Tool for Finding Significant Concurrent Annotations in Gene Lists. *Genome Biol.* **2007**, *8* (1), 1–8.

(33) The Ontology Consortium. The Gene Ontology Resource : 20 Years and Still GOing Strong. *Nucleic Acids Res.* **2019**, *47* (November 2018), 330–338.

(34) Ashburner, M.; Ball, C. A.; Blake, J. A.; Botstein, D.; Butler, H.; Cherry, J. M.; Davis, A. P.; Dolinski, K.; Dwight, S. S.; Eppig, J. T.; et al. Gene Ontology: Tool for the Unification of Biology. *Nat. Genet.* **2000**, *25* (may), 25–29.

(35) Tarca, A. L.; Draghici, S.; Khatri, P.; Hassan, S. S.; Mittal, P.; Kim, J.; Kim, C. J.; Kusanovic, J. P.; Romero, R.; Hall, S.; et al. A Novel Signaling Pathway Impact Analysis. *BIOINFORMATICS* **2009**, *25* (1), 75–82.

(36) Werner, D.; Hashimoto, S. Improved Working Model for Interpreting the Excitation Wavelength- and Fluence-Dependent Response in Pulsed Laser-Induced Size Reduction of Aqueous Gold Nanoparticles. *J. Phys. Chem. C* **2011**, *115* (12), 5063–5072.

(37) Pan, Y.; Neuss, S.; Leifert, A.; Fischler, M.; Wen, F.; Simon, U.; Schmid, G.; Brandau, W.; Jahnen-Dechent, W. Size-Dependent Cytotoxicity of Gold Nanoparticles. *Small* **2007**, *3* (11), 1941–1949.

(38) Tsoli, M.; Kuhn, H.; Brandau, W.; Esche, H.; Schmid, G. Cellular Uptake and Toxicity of Au55 Clusters. *Small* **2005**, *1* (8–9), 841–844.

(39) Encina, E. R.; Coronado, E. A. On the Far Field Optical Properties of Ag - Au Nanosphere Pairs. *J. Phys. Chem. C* **2010**, 16278–16284.

(40) Palik, E. *Handbook of Optical Constants of Solids*; Academic Press: New York, 1985.

SYNOPTIC TOC